

Supporting Information

In-situ activation induced surface reconstruction on Cr-incorporated Ni₃S₂ for enhanced alkaline hydrogen evolution reaction

Ruidi Li,^a Cong Chen,*^a Junxia Shen,^a Zhihe Wei,^b Pierre-Yves Olu,^c Wen Dong,^a Yang Peng,^b Ronglei Fan,*^a and Mingrong Shen*^a

^a School of Physical Science and Technology, Jiangsu Key Laboratory of Frontier Material Physics and Devices, Collaborative Innovation Center of Suzhou Nano Science and Technology, Soochow University, 1 Shizi Street, Suzhou 215006, China. E-mail addresses: cchen96@suda.edu.cn (C. Chen), rlfan@suda.edu.cn (R. Fan), mrshen@suda.edu.cn (M. Shen)

^b Soochow Institute of Energy and Material Innovations, College of Energy, Provincial Key Laboratory for Advanced Carbon Materials and Wearable Energy Technologies, Soochow University, Suzhou 215006, China

^c John Cockerill Hydrogen S.A, 1 Rue Jean Potier, 4100 Seraing, Belgium^c *John Cockerill Hydrogen S.A, 1 Rue Jean Potier, 4100 Seraing, Belgium*

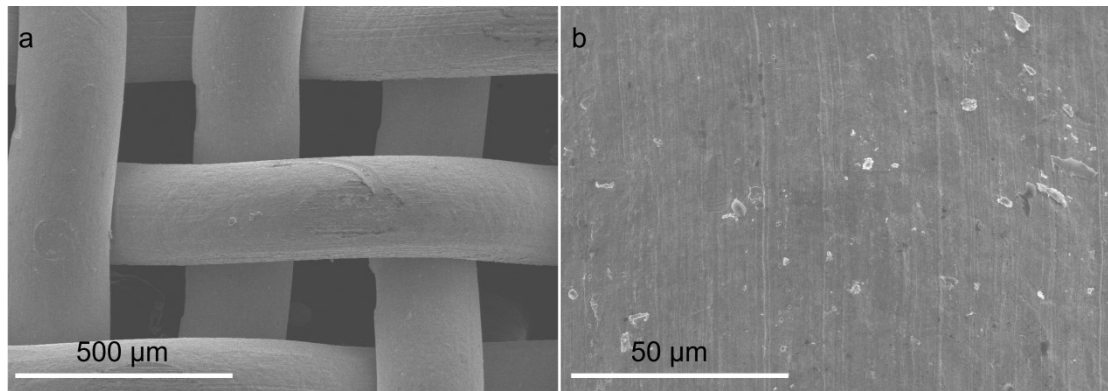


Fig. S1. SEM images of Ni mesh.

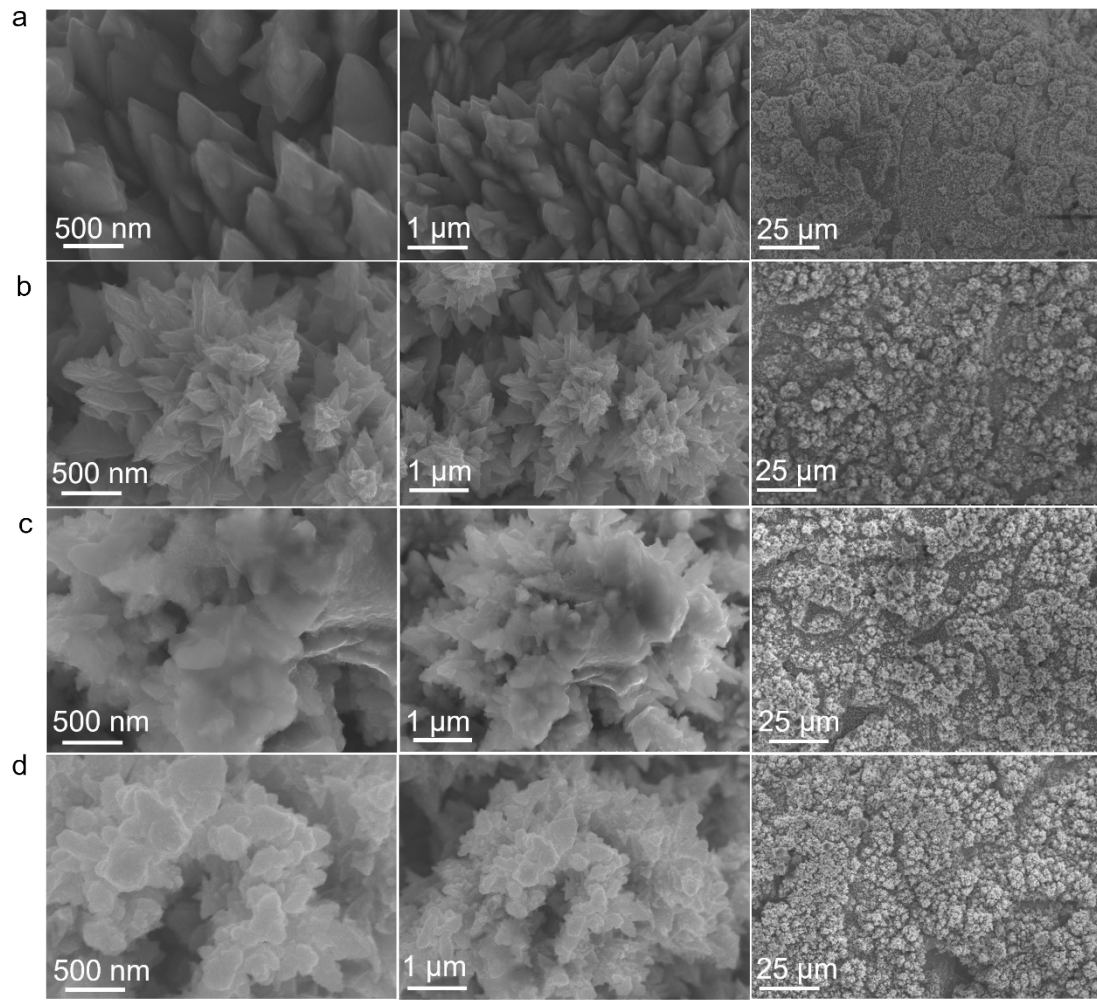


Fig. S2. SEM images of a) Ni₃S₂/NM, b) Cr-Ni₃S₂/NM, c) A- Ni₃S₂/NM and d) A-Cr- Ni₃S₂/NM at different magnifications.

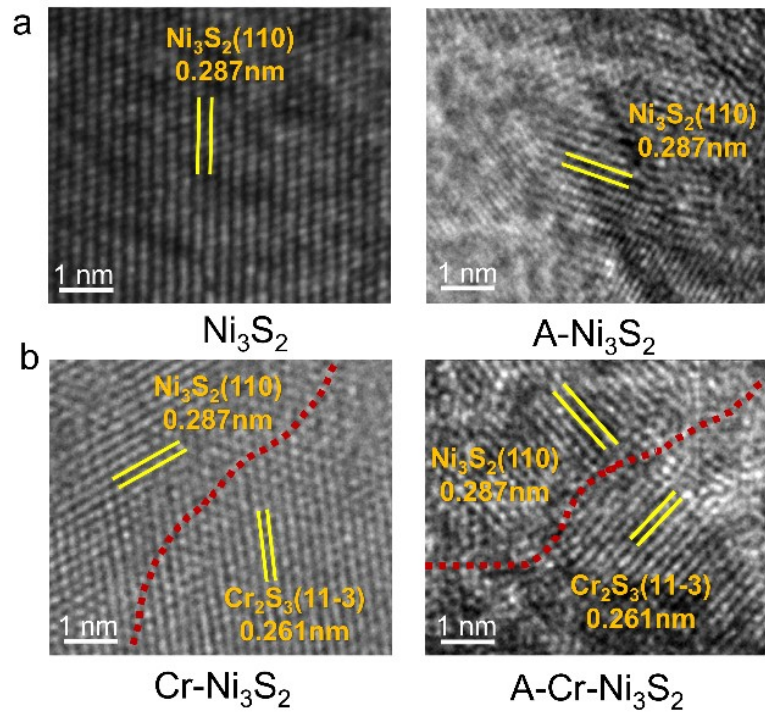


Fig. S3. a) Comparison of HRTEM images between Ni_3S_2 and $\text{A}-\text{Ni}_3\text{S}_2$, b) Comparison of HRTEM images between $\text{Cr}-\text{Ni}_3\text{S}_2$ and $\text{A}-\text{Cr}-\text{Ni}_3\text{S}_2$.

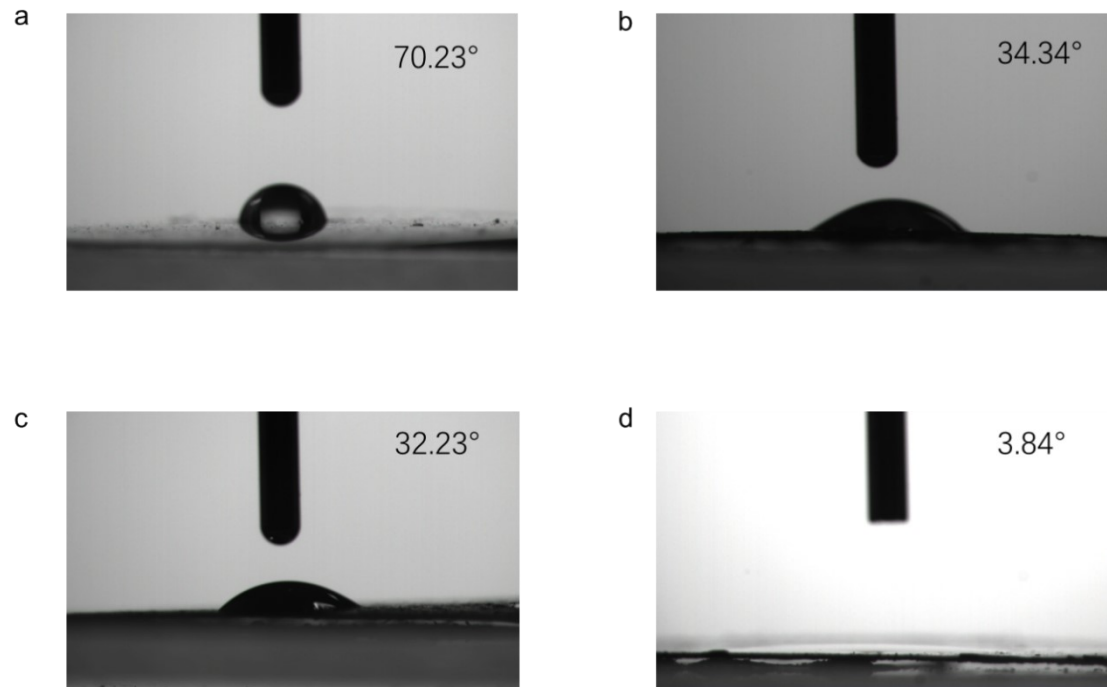


Fig. S4. Water contact angle of a) Ni_3S_2 , b) $\text{Cr}-\text{Ni}_3\text{S}_2$, b) $\text{A}-\text{Ni}_3\text{S}_2$, d) $\text{A}-\text{Cr}-\text{Ni}_3\text{S}_2$. (In this section, all samples were prepared on Ni sheet to assess the water contact angle)

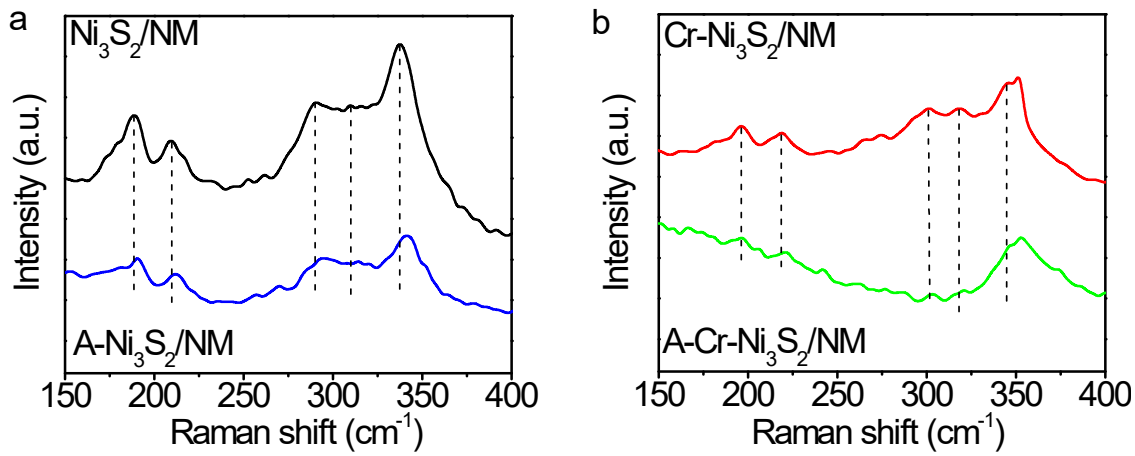


Fig. S5. Local magnification of Raman spectra of four samples.

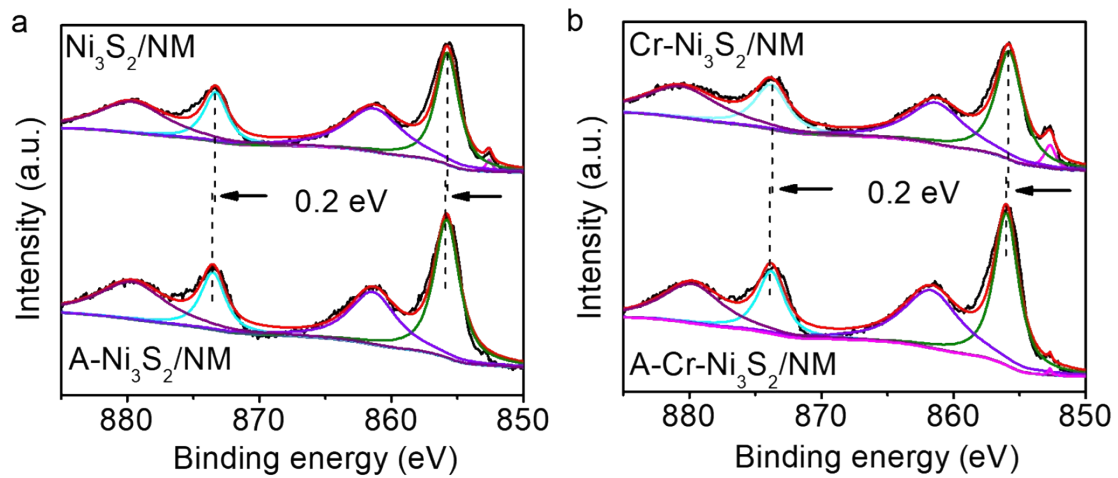


Fig. S6. XPS Ni 2p comparison of samples before and after activation.

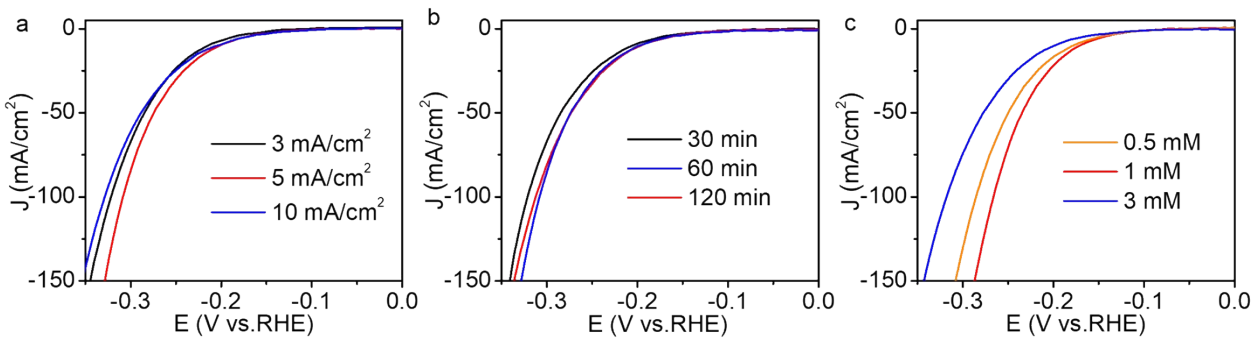


Fig. S7. a-b) the optimization process of $\text{Ni}_3\text{S}_2/\text{NM}$ based on current density and deposition time.
 c) the optimization process of $\text{Cr}-\text{Ni}_3\text{S}_2/\text{NM}$ based on different Cr concentrations in precursor solution.

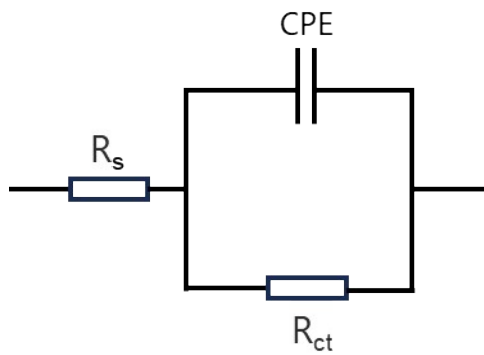


Fig. S8. The equivalent circuit model corresponding to the charge transfer from the Ni mesh to the electrolyte through $\text{Ni}_3\text{S}_2/\text{NM}$, $\text{Cr-Ni}_3\text{S}_2/\text{NM}$, $\text{A-Ni}_3\text{S}_2/\text{NM}$ and $\text{A-Cr-Ni}_3\text{S}_2/\text{NM}$ catalyst.

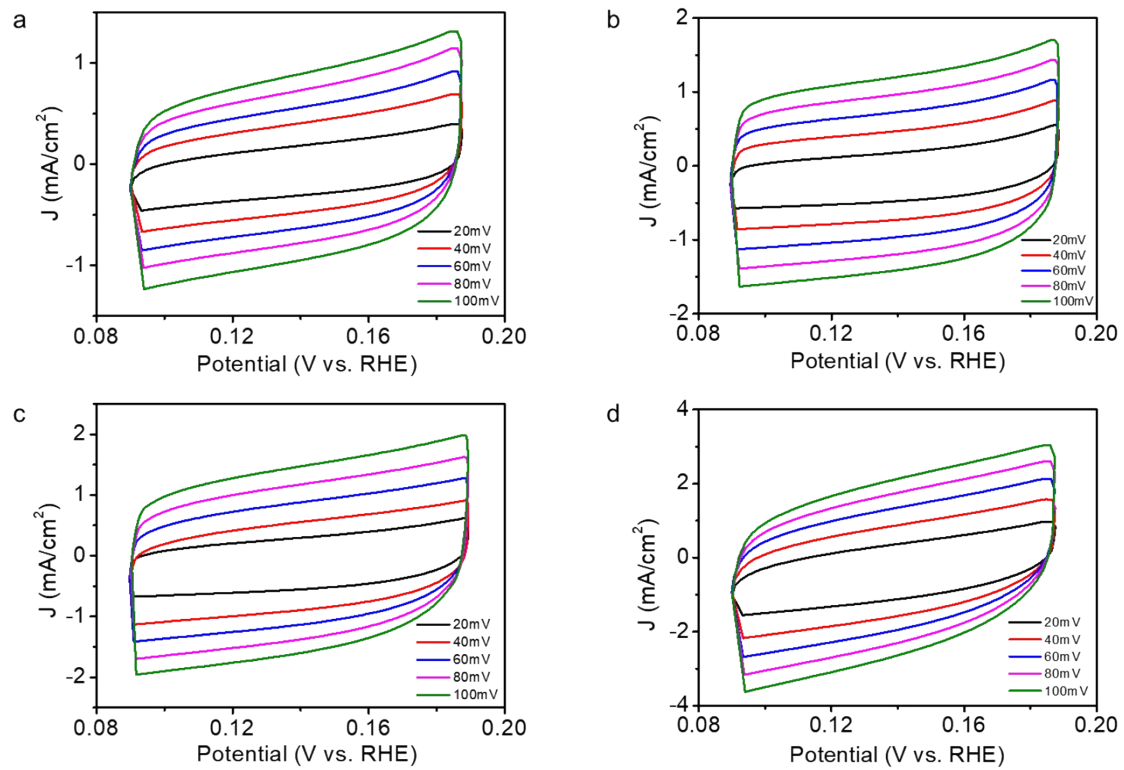


Fig. S9. Cyclic voltammetry for HER at the scan rates of 20, 40, 60, 80, and 100 mV/s in the range of no faradaic processes for a) Ni₃S₂/NM, b) Cr-Ni₃S₂/NM, c) A-Ni₃S₂/NM and d) A-Cr-Ni₃S₂/NM.

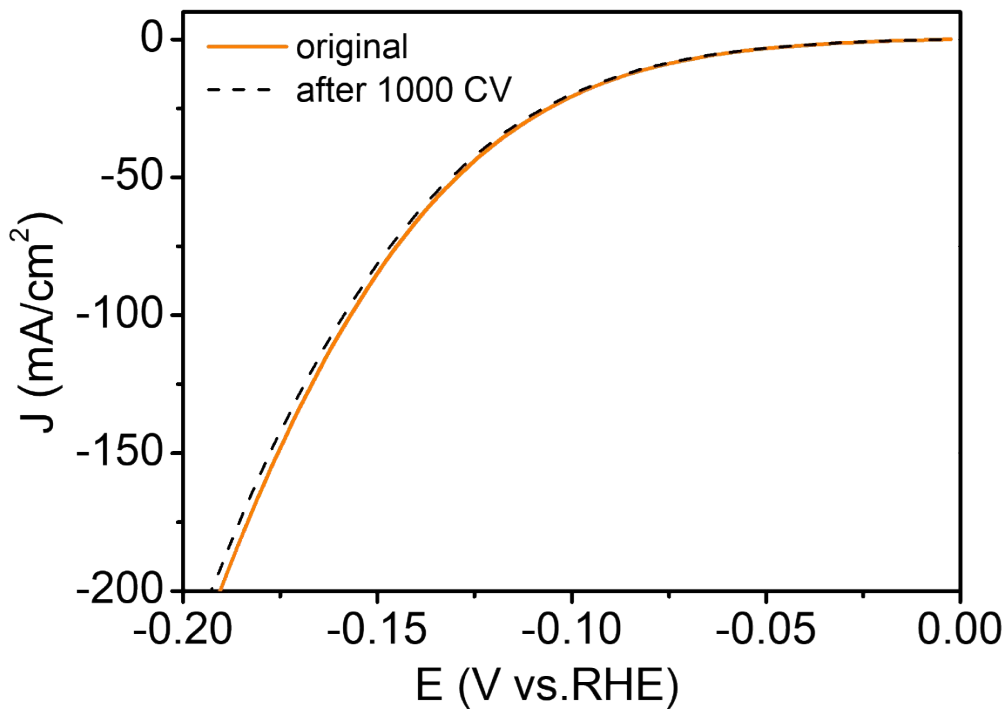


Fig. S10. Comparison of the LSV curves of A-Cr-Ni₃S₂/NM before and after 1000 CV cycles, respectively.

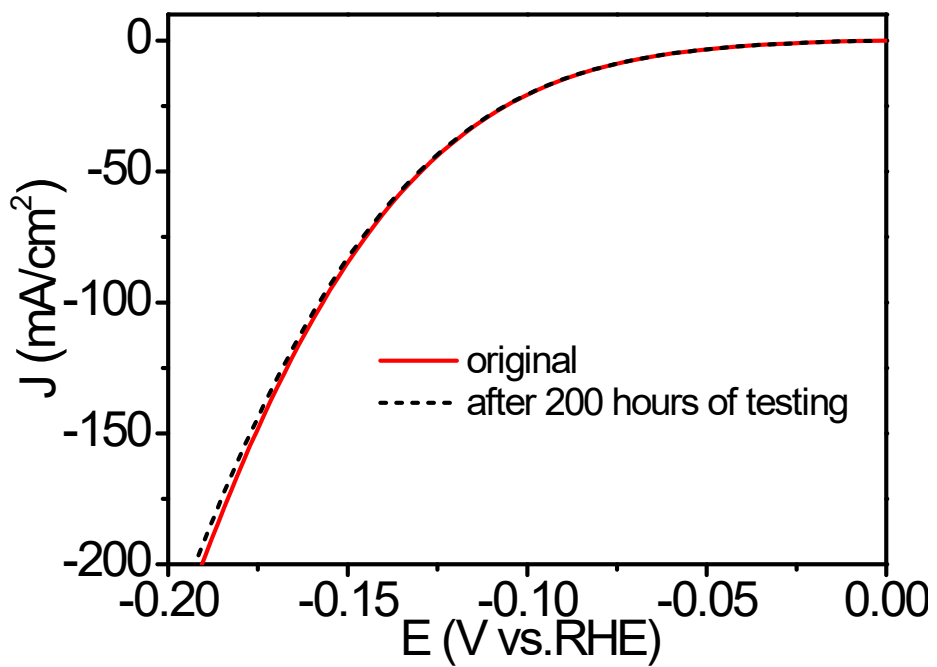


Fig. S11. Comparison of the LSV curves of A-Cr-Ni₃S₂/NM before and after 200 hours of testing, respectively.

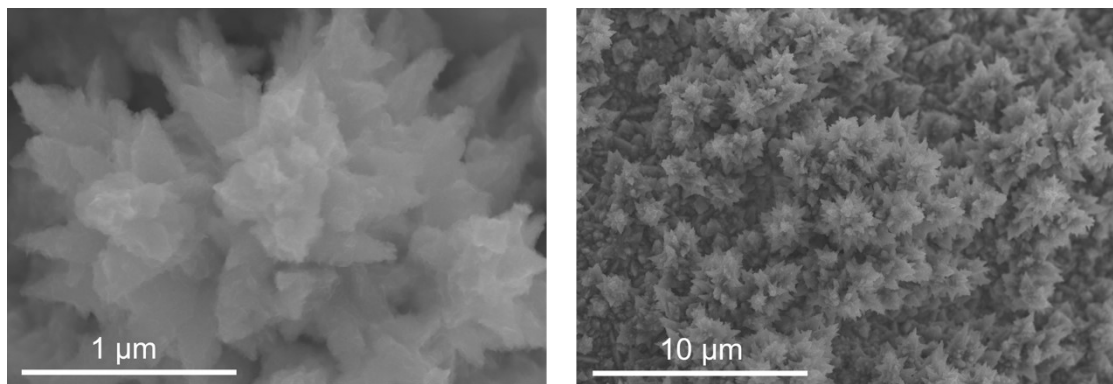


Fig. S12. The SEM of A-Cr-Ni₃S₂/NM after stability test.

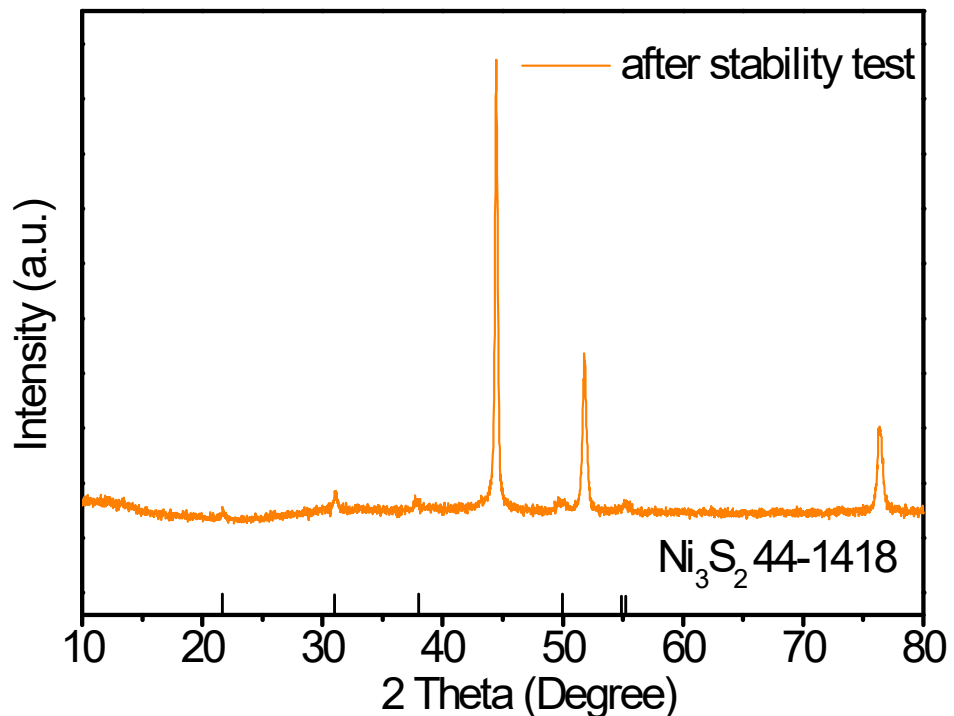


Fig. S13. The XRD pattern of A-Cr-Ni₃S₂/NM after stability test.

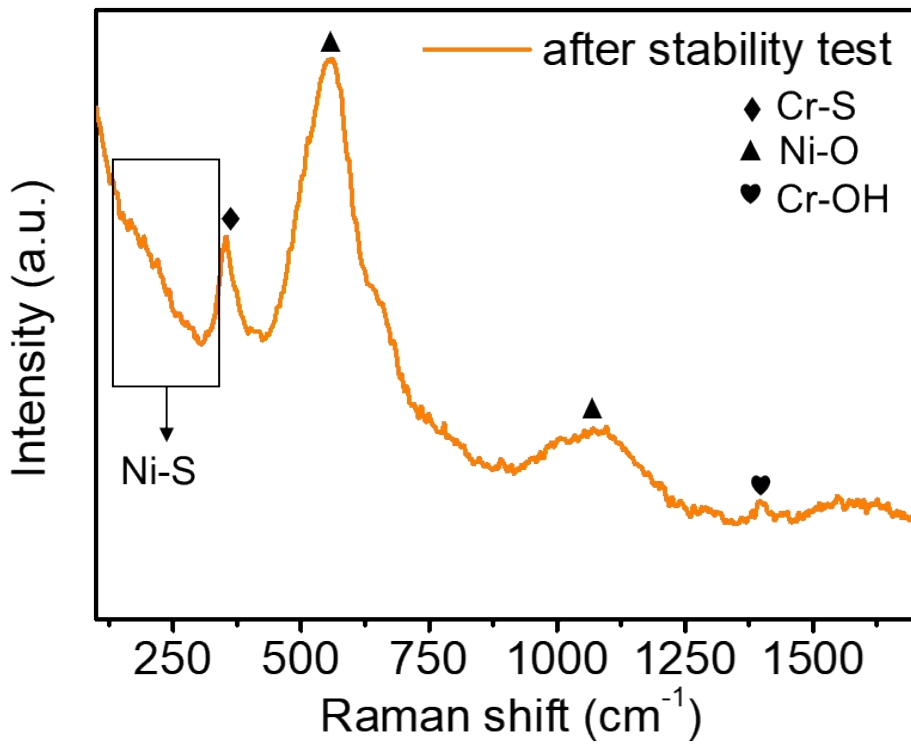


Fig. S14. The Raman pattern of A-Cr-Ni₃S₂/NM after stability test.

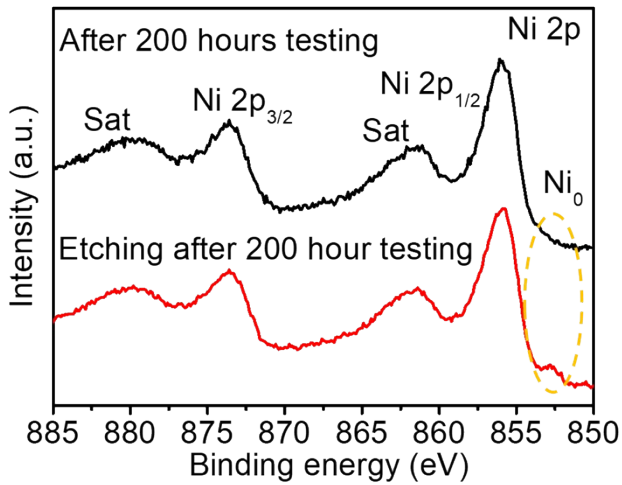


Fig. S15. Comparison of XPS Ni 2p spectra for A-Cr-Ni₃S₂ after stability testing and post-stability-test etching.

We characterized the XPS Ni 2p spectra for A-Cr-Ni₃S₂ after stability testing and depth profiling via Ar⁺ etching. The results indicate that the Ni⁰ in A-Cr-Ni₃S₂ disappears after stability testing and reappears after Ar⁺ etching, suggesting that the surface reconstruction after stability testing only occurs in a few nanometers area of the surface, and the overall structure of the A-Cr-Ni₃S₂ catalyst is very stable.

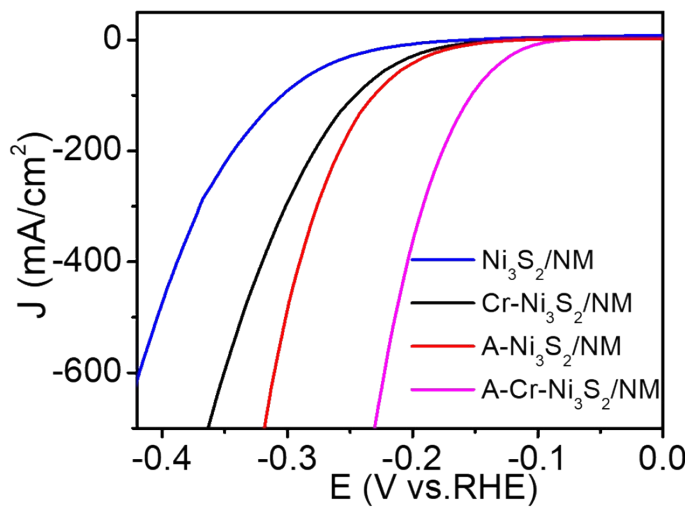


Fig. S16. LSV curves of different samples in 30 wt% KOH, 80°C.

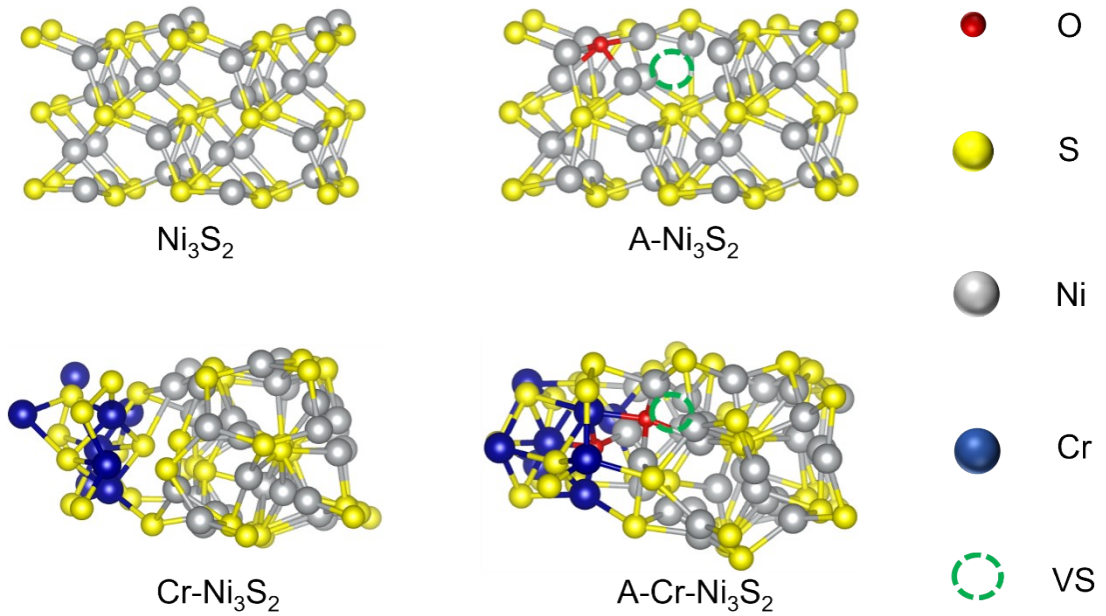


Fig. S17. Structure diagrams of Ni_3S_2 (110) and Cr_3S_2 (11-3) crystal faces of Ni_3S_2 , $\text{A}-\text{Ni}_3\text{S}_2$, $\text{Cr}-\text{Ni}_3\text{S}_2$, and $\text{A}-\text{Cr}-\text{Ni}_3\text{S}_2$.

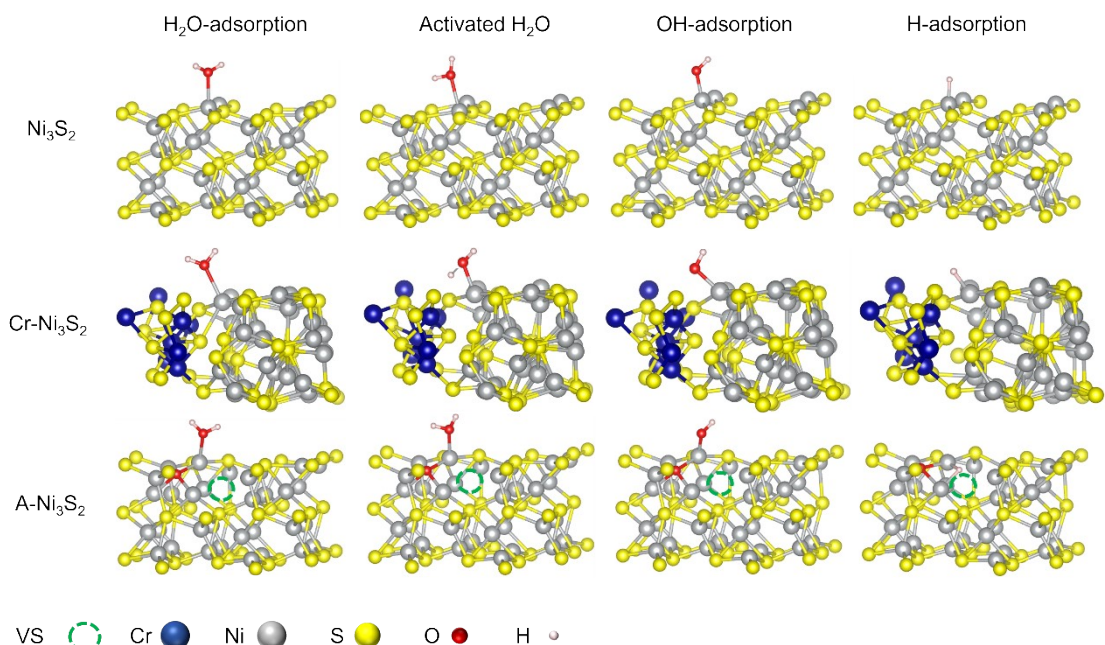


Fig. S18. The as-built structural models of Ni₃S₂, A-Ni₃S₂, Cr-Ni₃S₂, and A-Cr-Ni₃S₂ for different steps in alkaline HER.

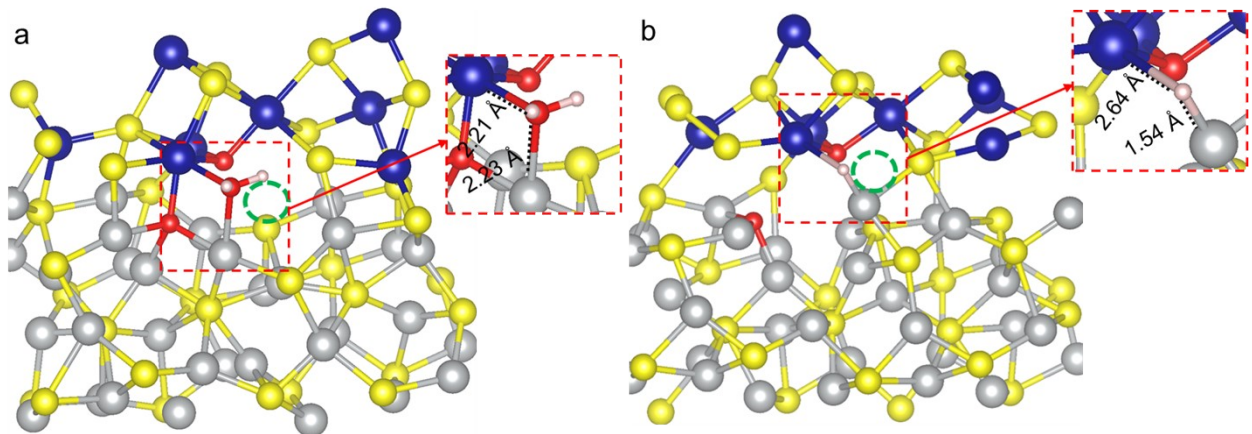


Fig. S19. Actual active sites of a) H₂O dissociation and b) H adsorption on A-Cr-Ni₃S₂ during the HER.

Table S1. Full width at half maxima (FWHM) of the diffraction peaks of Ni₃S₂(110) on various electrodes.

Sample	FWHM (°)
Ni ₃ S ₂ /NM	0.23
Cr-Ni ₃ S ₂ /NM	0.30
A-Ni ₃ S ₂ /NM	0.39
A-Cr-Ni ₃ S ₂ /NM	0.43

Table S2. The fitted value of charge transfer resistance for the Ni₃S₂/NM, Cr-Ni₃S₂/NM, A-Ni₃S₂/NM and A-Cr-Ni₃S₂/NM using the equivalent circuits.

Sample	R _s (Ω)	R _{ct} (Ω)
Ni ₃ S ₂ /NM	0.47	8.78
Cr-Ni ₃ S ₂ /NM	0.44	5.05
A-Ni ₃ S ₂ /NM	0.40	3.72
A-Cr-Ni ₃ S ₂ /NM	0.48	2.67

Table S3. Comparison of HER performance with some recently reported Ni S-based electrocatalysts in 1 M KOH, 25 °C.

Catalyst	Electrolyte	Overpotential [mV]	Current density [mA cm ⁻²]	Reference
NiS/Ni ₃ S ₂ @CC	1 M KOH	84	10	1
NiS/Ni ₂ S ₂ /CeO ₂	1 M KOH	85	10	2
4Cr-NiS _x /NF	1 M KOH	87	10	3
Mn-NiS/Mn-Ni ₃ S ₄	1 M KOH	94.2	10	4
A-MoS ₂ -Ni ₃ S ₂ -NF	1 M KOH	95	10	5
Au/Ni ₃ S ₂ /NF	1 M KOH	97	10	6
WS ₂ @graphene	1 M KOH	117	10	7
Ni _{1-x} Fe _x S ₂	1 M KOH	118	10	8
NiCo ₂ S ₄ /Ni ₃ S ₂	1 M KOH	119	10	9
MoS ₂ /Fe-Ni ₃ S ₂ /NF	1 M KOH	121	10	10
Cu NDs/Ni ₃ S ₂ NTs-CFs	1 M KOH	128	10	11
Ni ₃ S ₂ @NGCLs/NF	1 M KOH	134	10	12
NiWO ₄ /Ni ₃ S ₂ -16	1 M KOH	150	10	13
Ni ₃ S ₂ @Ni ₉ S ₈ core-shell	1 M KOH	178	10	14

Table S4. Gibbs free energy changes in different steps for various samples.

Sample	$* + \text{H}_2\text{O} \rightarrow \text{H}_2\text{O}^*$	$\text{H}_2\text{O}^* \rightarrow \text{H}_2\text{O}^*\text{TS}$	$\text{H}_2\text{O}^*\text{TS} \rightarrow \text{OH}^* + \text{H}^*$	$\text{H}^* \rightarrow 1/2 (\text{H}_2)$
	adsorption of H_2O	dissociation of H_2O		H_2 desorption
$\text{Ni}_3\text{S}_2/\text{NM}$	-0.44 eV	1.28 eV	-2.85 eV	0.50 eV
A- $\text{Ni}_3\text{S}_2/\text{NM}$	-0.23 eV	0.91 eV	-3.2 eV	0.31 eV
Cr- $\text{Ni}_3\text{S}_2/\text{NM}$	-0.18 eV	1.16 eV	-4.92 eV	0.43 eV
A-Cr- $\text{Ni}_3\text{S}_2/\text{NM}$	-0.46 eV	0.59 eV	-1.85 eV	0.15 eV

References

- 1 R.-C. Li, X.-Y. Zhang, Z.-Y. Qu, F.-Y. Liu, Q.-Q. Xu, Z.-X. Hu, J.-W. Li, M.-N. Ghazzal, J.-L. Yu, *Rare Met.* 2024, **43** (9), 4377-4386.
- 2 D. Xiang, Z. Qin, Y. Gan, X. Luo, X. Li, L. Hu, Y. Xin, X. Lv, M. Hu, S. Jiao, *Mater. Today Chem.* 2023, **34**, 101791.
- 3 D. Liu, R. Tong, Y. Qu, Q. Zhu, X. Zhong, M. Fang, K. Ho Lo, F. Zhang, Y. Ye, Y. Tang, S. Chen, G. Xing, H. Pan, *Appl. Catal. B* 2020, **267**, 118721.
- 4 H. Huang, X. Hu, Z. Hou, D. Yang, D. Xiang, L. Hu, *Fuel.* 2022, **328**, 125337.
- 5 M. Hu, Y. Qian, S. Yu, Q. Yang, Z. Wang, Y. Huang, L. Li, *Small* 2024, **20** (5), 2305948.
- 6 H. Liu, J. Cheng, W. He, Y. Li, J. Mao, X. Zheng, C. Chen, C. Cui, Q. Hao, *Appl. Catal. B* 2022, **304**, 120935.
- 7 W. Han, Z. Liu, Y. Pan, G. Guo, J. Zou, Y. Xia, Z. Peng, W. Li, A. Dong, *Adv. Mater.* 2020, **32** (28), 2002584.
- 8 Y. Sun, J. Wu, Z. Zhang, Q. Liao, S. Zhang, X. Wang, Y. Xie, K. Ma, Z. Kang, Y. Zhang, *Energy Environ. Sci.* 2022, **15** (2), 633-644.
- 9 H. Liu, X. Ma, Y. Rao, Y. Liu, J. Liu, L. Wang, M. Wu, *ACS Appl. Mater. Interfaces.* 2018, **10** (13), 10890-10897.
- 10 M. Dou, M. Yao, K. Ding, Y. Cheng, H. Shao, S. Li, Y. Chen, *Dalton Trans.* 2023, **52** (48), 18342-18353.
- 11 J.X. Feng, J.Q. Wu, Y.X. Tong, G.R. Li, *J. Am. Chem. Soc.* 2018, **140** (2), 610-617.
- 12 B. Li, Z. Li, Q. Pang, J.Z. Zhang, *Chem. Eng. J.* 2020, **401**.
- 13 S. Huang, Y. Meng, Y. Cao, F. Yao, Z. He, X. Wang, H. Pan, M. Wu, *Appl. Catal. B* 2020, **274**, 119120.
- 14 G. Zhao, Y. Xing, Y. Liu, X. Wang, B. Zhang, L. Mu, W. Liao, X. Xu, *Mater. Today Chem.* 2023, **34**, 101758.